



ARTICLE

A cyclic nucleotide-gated channel mediates cytoplasmic calcium elevation and disease resistance in rice

Jiachang Wang^{1,2}, Xi Liu¹, An Zhang³, Yulong Ren², Fuqing Wu², Gang Wang³, Yang Xu¹, Cailin Lei², Shanshan Zhu², Tian Pan¹, Yongfei Wang¹, Huan Zhang¹, Fan Wang¹, Yan-Qiu Tan³, Yupeng Wang², Xin Jin², Sheng Luo², Chunlei Zhou¹, Xiao Zhang¹, Jinling Liu², Shuai Wang², Lingzhi Meng², Yihua Wang¹, Xi Chen³, Qibing Lin², Xin Zhang², Xiuping Guo², Zhijun Cheng², Jiulin Wang², Yunlu Tian¹, Shijia Liu¹, Ling Jiang¹, Chuanyin Wu², Ertao Wang³, Jian-Min Zhou⁴, Yong-Fei Wang³, Haiyang Wang³ and Jianmin Wan²

The transient elevation of cytoplasmic calcium is essential for pathogen-associated molecular pattern (PAMP)-triggered immunity (PTI). However, the calcium channels responsible for this process have remained unknown. Here, we show that rice *CDS1* (*CELL DEATH and SUSCEPTIBLE to BLAST 1*) encoding OsCNGC9, a cyclic nucleotide-gated channel protein, positively regulates the resistance to rice blast disease. We show that OsCNGC9 mediates PAMP-induced Ca²⁺ influx and that this event is critical for PAMPs-triggered ROS burst and induction of PTI-related defense gene expression. We further show that a PTI-related receptor-like cytoplasmic kinase OsRLCK185 physically interacts with and phosphorylates OsCNGC9 to activate its channel activity. Our results suggest a signaling cascade linking pattern recognition to calcium channel activation, which is required for initiation of PTI and disease resistance in rice.

Cell Research (2019) 29:820–831; <https://doi.org/10.1038/s41422-019-0219-7>

INTRODUCTION

Plants are constantly challenged by various pathogenic pathogens (viruses, bacteria and fungi) and consequently, have evolved a two-tiered innate immune system to fend off pathogens: pathogen-associated molecular pattern (PAMP)-triggered immunity (PTI) and effector-triggered immunity (ETI).^{1,2} PTI is generally considered to confer weaker, but broad-spectrum disease resistance, whereas R gene-mediated ETI usually confers stronger race-specific disease resistance.³ PTI can be triggered via activation of plasma membrane (PM)-localized pattern recognition receptors (PRRs) by conserved pathogen-associated molecular patterns (PAMPs). Within minutes, pattern recognition triggers a set of signaling cascades, including increase of cytoplasmic calcium ([Ca²⁺]_{cyt}), induction of reactive oxygen species (ROS) and expression of PTI-related defense genes.⁴ Further, it has been demonstrated that pattern-triggered [Ca²⁺]_{cyt} burst is implemented by Ca²⁺ influx from apoplast and Ca²⁺ release from intracellular stores.⁵ However, despite that Ca²⁺ influx has been demonstrated to be a core event for triggering PTI,^{6,7} the channel proteins responsible for PAMP-mediated Ca²⁺ influx have remained elusive.^{8,9}

On the other hand, it was recently shown that after pattern recognition, PRRs directly link with members of receptor-like cytoplasmic kinase subfamily VII (RLCK VII) to initiate multiple downstream signaling pathways.⁹ For example, Arabidopsis RLCK member BIK1 transmits signals from FLS2 by phosphorylation of

RbohD during PTI.¹⁰ In rice, RLCK family members OsRLCK176 and OsRLCK185 interact with a rice PRR, OsCERK1, and are directly phosphorylated by OsCERK1 in a ligand-dependent manner.^{11–13} In line with this, the *Oslck176* mutant and *Oslck185* mutant show deficiencies in multiple pattern-induced immune responses, including ROS production, defense gene expression and MAPK activation.^{11,12} Although previous studies have shown that OsRLCK185 and OsRLCK176 mediate pattern-induced MAPK activation by interacting with OsCERK1, the underlying mechanisms by which rice RLCKs transmit signal to downstream signaling intermediates during PTI remain largely unclear.

Fungal pathogen *Magnaporthe oryzae* (*M. oryzae*) causes the most devastating disease that damages rice yield and grain quality worldwide.¹⁴ Several blast resistance genes encoding R proteins of the nucleotide-binding leucine-rich repeat (NLR) family have been identified, and they participate in ETI.^{15,16} On the other hand, accumulating evidence indicates PTI-mediated blast resistance also operates in rice.^{17–19} However, the signaling mechanisms governing PTI-mediated blast resistance in rice remain poorly understood.

The cyclic nucleotide-gated channels (CNGCs) gene family encodes a group of nonspecific, Ca²⁺-permeable cation channels.²⁰ Several Arabidopsis CNGCs (AtCNGCs) have been characterized electrophysiologically. For example, AtCNGC1 and AtCNGC2 are permeable to both K⁺ and Ca²⁺,^{21,22} and AtCNGC5, 6, 7, 8, 9, 10, 14, 16 and 18 have been shown to be Ca²⁺-permeable diverlant cation-selective channels.^{23–29} In rice,

¹National Key Laboratory for Crop Genetics and Germplasm Enhancement, Jiangsu Plant Gene Engineering Research Center, Nanjing Agricultural University, Nanjing 210095, China; ²National Key Facility for Crop Gene Resources and Genetic Improvement, Institute of Crop Sciences, Chinese Academy of Agricultural Sciences, Beijing 100081, China; ³National Key Laboratory of Plant Molecular Genetics, Institute of Plant Physiology and Ecology, CAS Center for Excellence in Molecular Plant Sciences, Chinese Academy of Sciences, Shanghai 200032, China and ⁴The State Key Laboratory of Plant Genomics, Institute of Genetics and Developmental Biology, Chinese Academy of Sciences, Beijing 100101, China

Correspondence: Jianmin Wan (wanjm@njau.edu.cn)

These authors contributed equally: Jiachang Wang, Xi Liu, An Zhang

Received: 25 June 2019 Accepted: 1 August 2019

Published online: 23 August 2019

OscNGC13 was also identified as a Ca^{2+} -permeable divergent cation-selective channel.³⁰ CNGCs have been shown to be involved in numerous physiological processes in plants, including immune responses, pollen tube germination and elongation, stomatal movement and root gravitropism.³¹ For example, the Arabidopsis *defense-no-death* (*dnd1*) mutant was identified as a mutant for *AtCNGC2* and the *constitutive expresser of pathogenesis-related (PR) genes22* (*cpr22*) mutant was shown to be caused by a genomic deletion, resulting in an in-frame chimeric *AtCNGC11-AtCNGC12* fusion.^{32,33} Although the effects of CNGCs on *R*-gene-mediated and damage associated molecular pattern (DAMP)-induced immune responses have been reported, little is known about their role in plant PTI signaling pathway.⁸

In this study, we report the isolation and mechanistic characterization of a rice mutant, *cds1* (*cell death and susceptible to blast 1*), which displayed impaired blast resistance at the seedling stage. *CDS1* encodes a rice CNGC protein, OsCNGC9. The OsCNGC9-mediated Ca^{2+} influx is important for PAMPs-induced signaling events, including ROS burst and PTI-related gene expression. Further analysis indicates that rice PTI signal transducer, OsRLCK185, physically interacts with and phosphorylates OsCNGC9 to activate its channel activity. Together, these findings provide novel mechanistic insights into the regulatory mechanisms of OsCNGC9 and suggest a signaling cascade linking PAMPs recognition to OsCNGC9-mediated Ca^{2+} influx to trigger PTI in plants.

RESULTS

The *cds1* mutant plants show impaired blast resistance at the seedling stage and lesion-mimic phenotype after flowering. In order to identify new genes involved in the regulation of rice disease resistance, we isolated a stable natural mutant *cds1* with enhanced susceptibility to rice blast from the progenies derived from the cross of two *japonica* cultivars, Ningjing1 and Yun2273. Although *cds1* seedlings were completely normal in morphology (Supplementary information, Fig. S1a), blast resistance assay revealed that they were significantly more susceptible to rice blast than wild type (WT) seedlings. After inoculating with blast, the lesion length and relative fungal growth of punch-inoculated leaves of WT seedlings were obviously lower than those of *cds1* seedlings (Fig. 1a–c). Interestingly, *cds1* leaves developed spontaneous cell death, examined by trypan blue staining (an indicator of programmed cell death, PCD), and measurement of chlorophyll contents after flowering (Supplementary information, Fig. S1b–f). qRT-PCR analysis showed that the expression of a representative cell death marker gene (*OsNAC4*) was significantly up-regulated in the *cds1* mutants (Supplementary information, Fig. S1g). These observations suggest that *CDS1* is a positive regulator of rice innate immunity at the seedling stage, but its genetic lesion can trigger spontaneous PCD after flowering, a phenomenon common to many important immune proteins.^{1,34}

CDS1 encodes a CNGC

Genetic analysis revealed that the lesion mimic phenotype of *cds1* was controlled by a single recessive nuclear gene (Supplementary information, Table S1). The *CDS1* locus was mapped to a 40-kb genomic region flanked by the markers PCD-22 and PCD-27 using a large F2 mapping population developed by crossing *cds1* with the *indica* cultivar 9311 (Fig. 1d). Sequence analysis revealed a 4-bp deletion in the coding region of LOC_Os09g38580, but no mutation was detected in other genes contained in the fine mapping region (Fig. 1e). LOC_Os09g38580 was predicted to encode a cyclic nucleotide-gated channel with six transmembrane domains, a pore-forming region and a CNBD domain at the C-terminal region (Fig. 1f) and it was previously named OsCNGC9.³⁵ The 4-bp deletion was predicted to introduce a premature stop codon, resulting in translation of only the first 5 transmembrane domains in *cds1* (designated *OsCNGC9-cds1* hereafter) (Fig. 1f).

To verify that LOC_Os09g38580 corresponds to the *CDS1* gene, we performed a genetic complementation assay. The transgene including the entire coding region of LOC_Os09g38580 with its native promoter (*pGOsCNGC9*) fully rescued the impaired blast resistance phenotype at the seedling stage and the spontaneous cell death phenotype of *cds1* after flowering in all positive transgenic lines (Fig. 1g–i, Supplementary information, Fig. S1h–k). These results confirmed that LOC_Os09g38580 (*OsCNGC9*) is the underlying gene for *CDS1*.

The expression pattern and protein properties of *OsCNGC9* qRT-PCR analysis showed that *OsCNGC9* was expressed in all tissues examined, with relatively higher expression in leaves (Supplementary information, Fig. S2a). The expression pattern was further verified by histochemical staining of the transgenic rice carrying a β -glucuronidase (GUS) reporter driven by the endogenous *OsCNGC9* promoter (Supplementary information, Fig. S2b–g). Further, the preferential expression of *OsCNGC9* in leaf mesophyll cells was confirmed using RNA in situ hybridization (Supplementary information, Fig. S2h, i).

Multiple sequence alignment and phylogenetic analysis showed that *OsCNGC9* is conserved in both dicots and monocots (Supplementary information, Fig. S3a, b). Transient expression of the *P35S:OsCNGC9-GFP* construct in the rice protoplasts showed that *OsCNGC9* was exclusively localized to the plasma membrane (Supplementary information, Fig. S4a–d). Similar result was also observed in stable transgenic rice expressing *OsCNGC9-GFP* driven by the *OsCNGC9* native promoter (Supplementary information, Fig. S4e–h). Yeast two-hybrid (Y2H) assay and bimolecular fluorescence complementation (BiFC) assay revealed that *OsCNGC9* could form homo-complex (Supplementary information, Fig. S4i, j), consistent with the earlier report that some CNGC isoforms can form homo-complex in *planta*.³⁶

OsCNGC9 is a Ca^{2+} -permeable divalent cation-selective inward channel

To analyze the ion permeability and selectivity of *OsCNGC9*, we first tested the accumulation of 9 different ions in *Escherichia coli* (*E. coli*) transiently expressing *OsCNGC9*. The contents of Ca^{2+} , Na^+ , K^+ , Mg^{2+} , Mn^{2+} , Fe^{2+} , Cu^{2+} , Zn^{2+} and Ni^{2+} were measured using inductively coupled plasma atomic-emission spectroscopy (ICP-AES). The results showed that the relative intracellular contents of Na^+ , K^+ and Mg^{2+} were decreased lightly, whereas the content of Ca^{2+} was significantly increased in *E. coli* expressing *OsCNGC9* relative to the control (Fig. 2a), suggesting that *OsCNGC9* could be Ca^{2+} selective relative to other cations. In support of this notion, intracellular Ca^{2+} accumulation was completely abolished by the application of 100 μM external gadolinium (Gd^{3+}), a well-known Ca^{2+} channel blocker (Fig. 2b). We next tested the external [Ca^{2+}]- and time-dependence of intracellular Ca^{2+} accumulation in *E. coli*, and observed strong intracellular Ca^{2+} accumulation in an external [Ca^{2+}]- and time-dependent manner (Fig. 2c, d). Similar cytosolic Ca^{2+} increase was observed in intact HEK293T cells expressing wild type *OsCNGC9*, but not in HEK293T cells expressing *OsCNGC9-cds1*, upon the application of 10 mM external CaCl_2 (Fig. 2e, f). Additionally, whole-cell patch clamping experiments showed large inward channel currents in HEK293T cells expressing wild type *OsCNGC9* in 10 mM Ca^{2+} bath solution, but only tiny background conductance was observed in HEK293T cells expressing *OsCNGC9-cds1* and the mock control under the same condition (Fig. 2g, h). Notably, we observed that the large *OsCNGC9*-mediated inward whole-cell currents were abolished by removal of external 10 mM Ca^{2+} (Supplementary information, Fig. S5a, b), demonstrating a clear dependence of external Ca^{2+} for *OsCNGC9*-mediated inward whole-cell currents. However, the whole-cell currents were relatively small (<100 pA), which precluded us from accurately measuring the shift of reversal

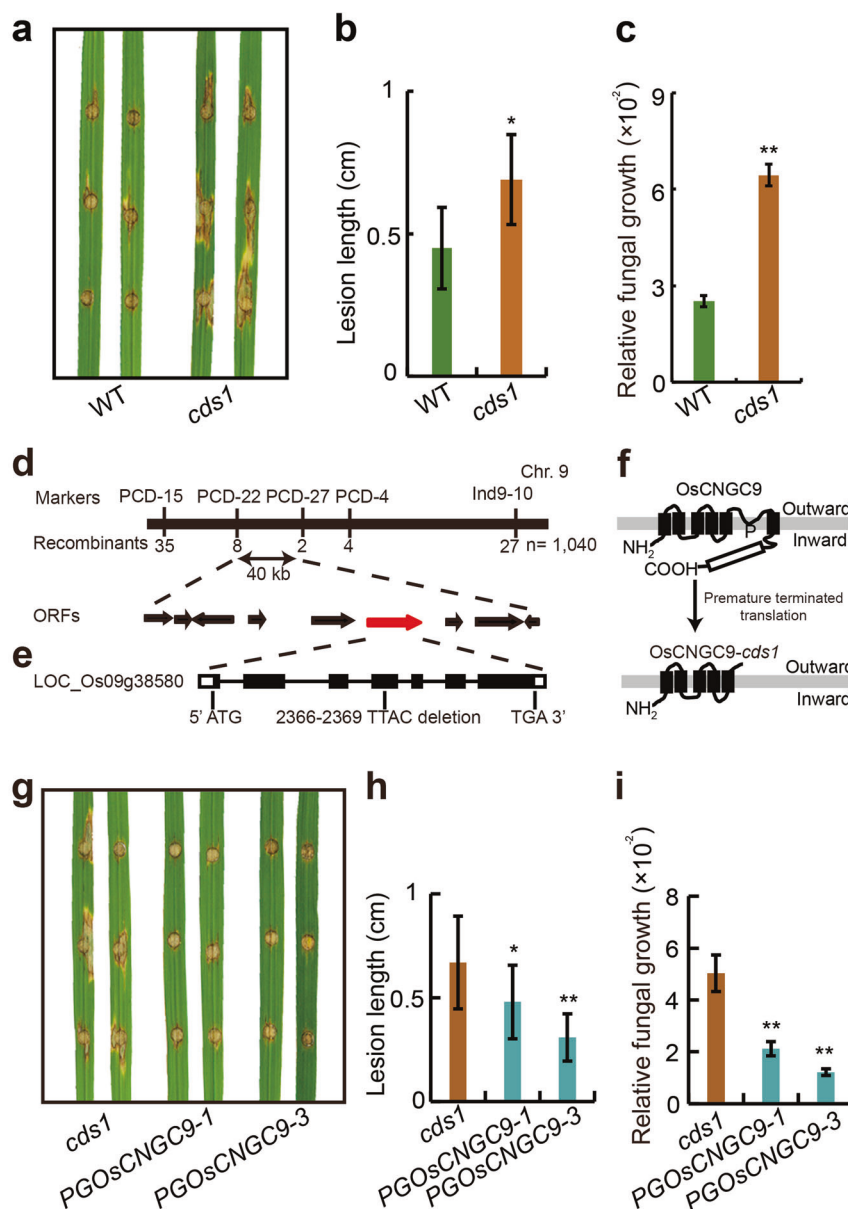


Fig. 1 The mutation in *OsCNGC9* is responsible for impaired blast resistance. **a** The *cds1* mutant plants are more susceptible to blast at the seedling stage (blast isolate 2015-412 was used for inoculation). **b, c** Lesion length (**b**) and relative fungal growth (**c**) of WT and *cds1* plants after punch inoculation with the blast. **d** Fine mapping of *OsCNGC9*. **e** Gene structure and the mutation site in *OsCNGC9*. **f** Schematic diagram of *OsCNGC9* secondary structure prediction. **g** pGOsCNGC9 rescues the seedling blast susceptibility phenotype of the *cds1* plants. **h, i** Lesion length (**h**) and relative fungal growth (**i**) of *cds1* and two pGOsCNGC9 transgenic lines after inoculation with the blast. WT, a normal sibling segregated from the stable progeny of the same cross between *japonica* Ningjing1 and *japonica* Yun2273. Values are means \pm SD (**b, h**, $n = 10$ samples; **c, i**, $n = 3$ replicates). WT control is only shown in (**a**) for simplicity. The Student's *t*-test analysis indicates a significant difference (* $P < 0.05$, ** $P < 0.01$)

potential upon the change of external Ca^{2+} concentration. Thus, we further tested the effect of Ca^{2+} channel blockers (La^{3+} and Gd^{3+}), and found that the application of either one of these two Ca^{2+} channel blockers could completely abolish *OsCNGC9*-mediated inward whole-cell currents in 10 mM Ca^{2+} bath solution (Supplementary information, Fig. S5c, d). Together, these results demonstrate that *OsCNGC9* functions as an inward Ca^{2+} channel, and the mutation in *cds1* disrupts its calcium channel activity.

It has been reported that some plant plasma membrane Ca^{2+} -permeable channels show similar permeability to Ba^{2+} and Ca^{2+} ,²⁴ we thus analyzed the permeability of *OsCNGC9* to Ba^{2+} . We replaced 10 mM Ca^{2+} in the bath solution with Ba^{2+} of the

same concentration, and observed large inward channel currents in HEK293T cells expressing *OsCNGC9* (Supplementary information, Fig. S5e, f), similar to *OsCNGC9*-mediated large inward currents recorded in 10 mM Ca^{2+} bath solution. Considering that some AtCNGCs are permeable to both Ca^{2+} and K^+ ,²¹ we also tested whether *OsCNGC9* is permeable to monovalent cations. Patch clamping experiments in HEK293T cells using K^+ -based bath and pipette solutions showed large inward K^+ channel currents in HEK293T cells expressing the well-characterized typical inward K^+ channel AtKAT1,³⁷ but only a tiny background conductance in HEK293T cells expressing *OsCNGC9* (Supplementary information, Fig. S5g, h). Thus, *OsCNGC9* does not have obvious permeability to monovalent K^+ .

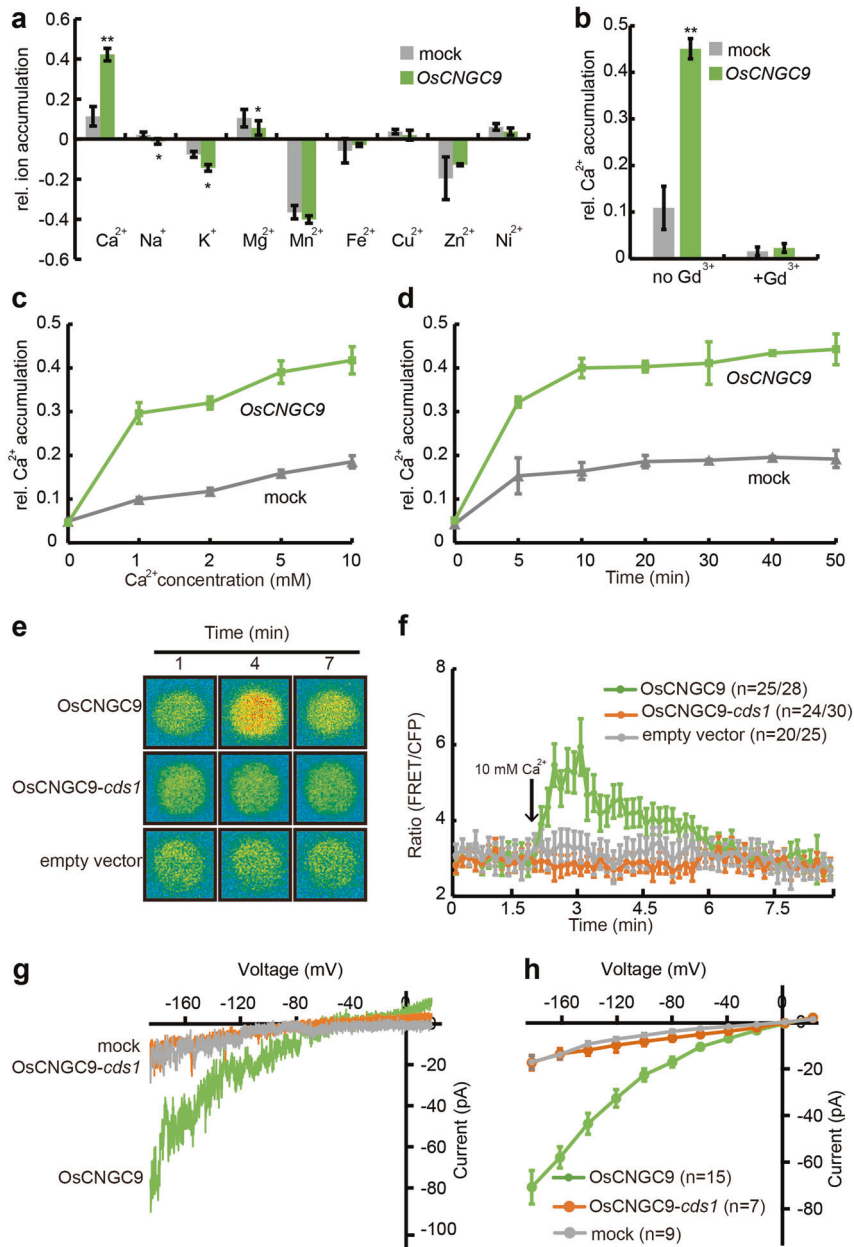


Fig. 2 *OsCNGC9* is a Ca^{2+} -permeable divalent cation-selective inward channel. **a** ICP-AES measurement of the intracellular contents of various ions in *E. coli* expressing *OsCNGC9*. **b** Accumulation of intracellular Ca^{2+} in *E. coli* expressing *OsCNGC9* after calcium channel blocker Gd^{3+} (0.1 mM) treatment. **c, d** The external $[\text{Ca}^{2+}]$ -dependent (**c**) and time-dependent (**d**) accumulation of intracellular Ca^{2+} in *E. coli* expressing *OsCNGC9*. **e, f** Typical fluorescent images (**e**) and average fluorescent intensity changes (**f**) in HEK293T cells expressing *OsCNGC9* or *OsCNGC9-cds1*. The two numbers in parentheses indicate the number of cells with the representative calcium pattern versus the number of total cells analyzed. **g, h** Typical whole-cell recordings (**g**) and the average current-voltage relationship (**h**) of patch clamping results in HEK293T cells expressing *OsCNGC9* or *OsCNGC9-cds1*. Values are means \pm SD (**a–d**, $n = 3$ replicates). The Student's *t*-test analysis indicates a significant difference ($*P < 0.05$, $**P < 0.01$)

OsCNGC9 is required for Ca^{2+} influx, ROS burst and PTI-related genes expression in response to PAMPs

We next investigated whether *OsCNGC9* can mediate Ca^{2+} influx in PTI by measuring the dynamics of Ca^{2+} flux in mesophyll cells after treatment with two PAMPs (chitin or flg22) in vivo using a Non-invasive Micro-test Technique. Previous studies have shown that these PAMP elicitors can trigger PTI signaling in plants.^{38,39} In response to chitin or flg22 stimulation, WT mesophyll cells, but not *cds1* mesophyll cells, exhibited robust and fast Ca^{2+} influx (Fig. 3a, b and Supplementary information, Fig. S6). These results suggest that *OsCNGC9* can mediate Ca^{2+} influx in rice PTI and this ability is impaired in the *cds1* mutants.

Pattern-induced Ca^{2+} influx precedes and is required for a number of signaling events including ROS burst in PTI.⁴⁰ We thus used a chemical luminescence assay to test whether PAMPs-triggered ROS burst is impaired in the *cds1* mutants. The ROS production level was higher in WT leaves than that in *cds1* after treatment with chitin or flg22. ROS level peaked about 11 min after chitin or flg22 treatments (Fig. 3c, d). In addition, qRT-PCR analysis showed that in response to flg22 or chitin treatments, the induction levels of two PTI-related defense genes (*KS4* and *PAL*) were notably lower in the *cds1* mutants compared to WT plants (Fig. 3e, f). These results suggest that *OsCNGC9* participates in the regulation of rice PTI.

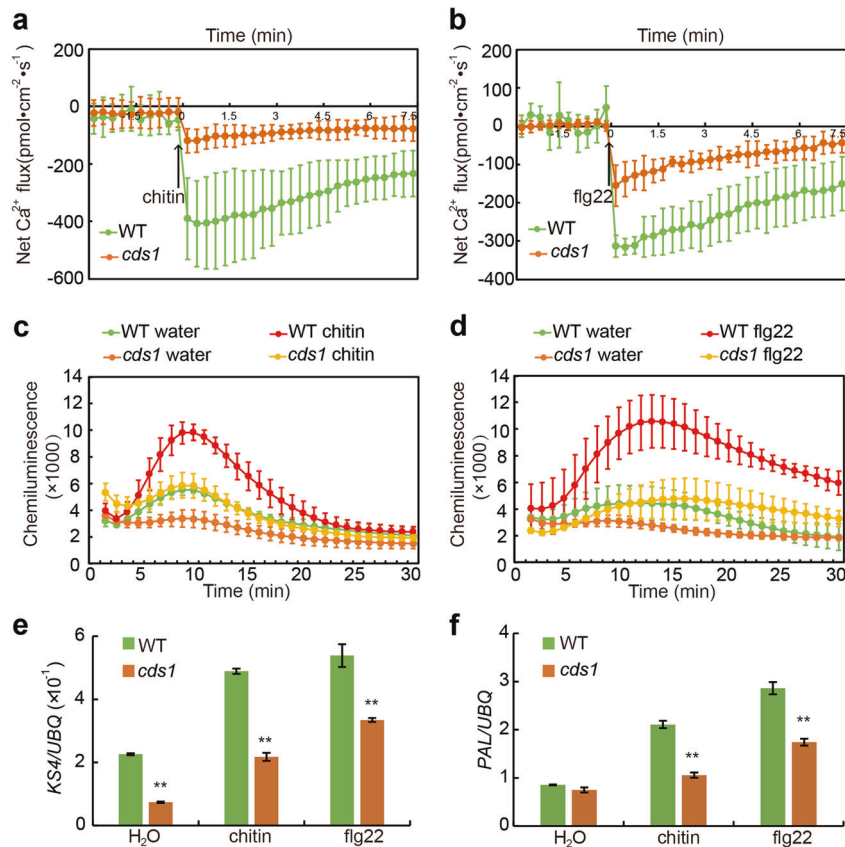


Fig. 3 OsCNGC9 is required for Ca^{2+} influx, ROS burst and PTI-related defense genes expression in response to PAMPs. **a, b** Comparison of calcium influx in mesophyll cells from WT and *cds1* plants after chitin (**a**) or flg22 (**b**) treatments. **c, d** Dynamic analysis of chitin (**c**) and flg22-induced (**d**) ROS generation in WT and *cds1* leaves. **e, f** The expression levels of two PTI-related defense genes (*KS4* and *PAL*) after treatment with chitin or flg22 in WT and *cds1* plants. Values are means \pm SD (**a, b**, $n = 6$ replicates; **c-f**, $n = 3$ replicates). The Student's *t*-test analysis indicates a significant difference (** $P < 0.01$)

OsRLCK185 physically interacts with and phosphorylates OsCNGC9 to activate its channel activity

Recent studies have shown that PRRs and members of RLCK VII play important roles in regulating plant innate immunity.⁹ To investigate the functional relationship between OsCNGC9 and PRRs/RLCKs, we performed yeast two-hybrid (Y2H) assay and luciferase complementation assay to test potential protein–protein interaction between OsCNGC9 with four rice PRRs and two RLCKs that have been previously reported to be involved in PTI.⁴ Both assays showed that OsCNGC9 could interact with three of them, including OsFLS2, OsRLCK176 and OsRLCK185 (Fig. 4a, b and Supplementary information, Fig. S7a, b). It has been shown that RLCKs, BIK1 and PBL1 act upstream of calcium channels in Arabidopsis.^{10,41} Y2H assay showed that OsCNGC9 interacts with OsRLCK176 and OsRLCK185 via its C-terminus (Supplementary information, Fig. S7c, d). Thus, we examined whether OsRLCK176 and OsRLCK185 can phosphorylate OsCNGC9 using an *in vitro* phosphorylation assay. The results showed that only OsRLCK185 could effectively phosphorylate the C-terminus of OsCNGC9 (Fig. 4c). These results suggest that OsRLCK185 is likely a regulator of OsCNGC9 during rice PTI. In support of this notion, co-immunoprecipitation assay confirmed the interaction between OsCNGC9 and OsRLCK185 in rice protoplasts (Fig. 4d).

We next investigated the effect of OsRLCK185 on the Ca^{2+} channel activity of OsCNGC9 expressed in HEK293T cells. A stronger cytosolic Ca^{2+} increase was observed in intact HEK293T cells coexpressing OsCNGC9 and OsRLCK185 upon application of 10 mM external CaCl_2 , but not in intact HEK293T cells coexpressing OsCNGC9 and OsRLCK185-K108E (an

inactive form of OsRLCK185¹²) (Fig. 4e). In addition, no significant cytosolic Ca^{2+} increase was observed in the HEK293T cells expressing either OsRLCK185 or OsRLCK185-K108E alone (Supplementary information, Fig. S7e). To further verify pattern-induced phosphorylation of OsCNGC9 C-terminus *in vivo*, we developed a phos-tag assay. A chitin-induced band-shift of the C-terminal fragment of OsCNGC9 was observed in wild type (Kitaake) protoplasts, but not in *Oscerk1* knockout mutant protoplasts (Fig. 4f and Supplementary information, Fig. S7f). These data collectively suggest that phosphorylation of OsCNGC9 by OsRLCK185 leads to activation of the OsCNGC9 channel activity and Ca^{2+} influx in response to PAMP.

Osr185/55 double mutant plants show impaired blast resistance and reduced pattern-induced Ca^{2+} influx

We next tested whether OsRLCK185 plays a role in regulating rice blast resistance. To avoid potential functional redundancy,¹² we conducted a blast resistance assay using *Osr185* and *Osr185/55* (a close homologous gene of OsRLCK185, which shares 84% amino acid identity with OsRLCK185⁴²) double mutant plant (Fig. 5a). After inoculating with blast, the lesion length and relative fungal growth of punch-inoculated leaves of *Osr185/55* double mutant seedlings were obviously higher than those of the corresponding wild type (Nipponbare) seedlings (Fig. 5b–d). Ca^{2+} flux assay showed that in response to chitin stimulation, Nipponbare mesophyll cells, but not *Osr185/55* double mutant mesophyll cells, exhibited fast Ca^{2+} influx (Fig. 5e). Moreover, no significant Ca^{2+} influx was observed after chitin treatment of the *Oscerk1* knockout mutant (Fig. 5f). These results together suggest that

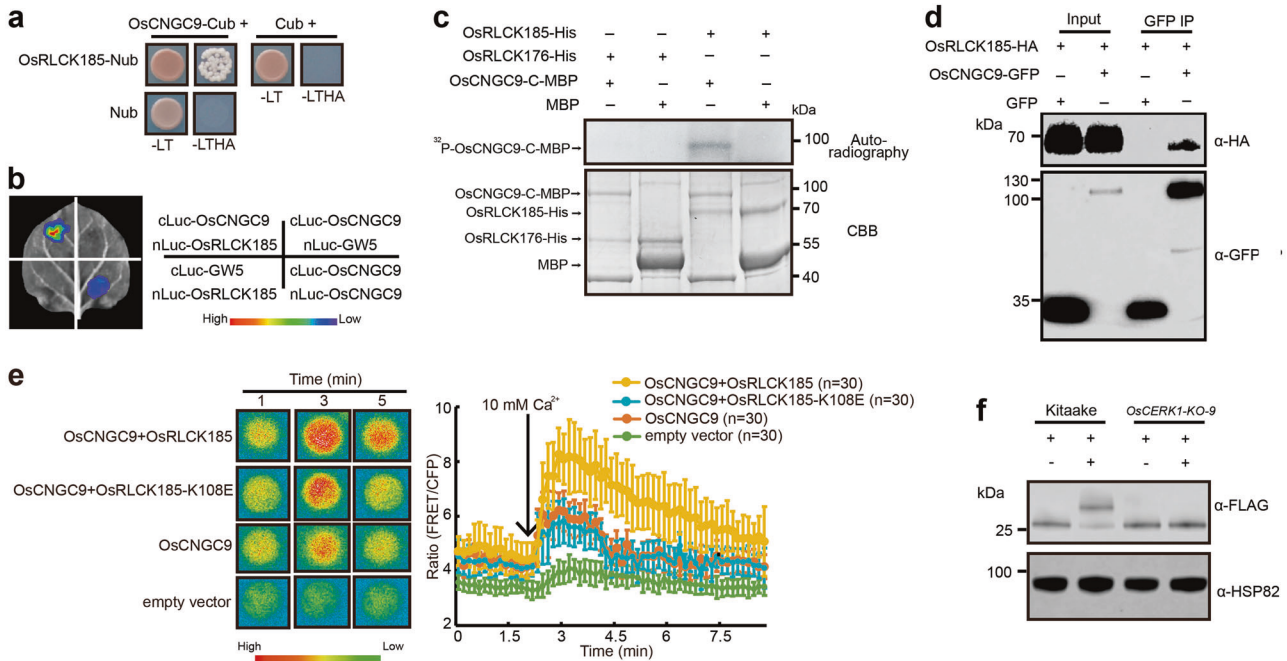


Fig. 4 OsRLCK185 physically interacts with and phosphorylates OsCNGC9 to activate its channel activity. **a** OsCNGC9 interacts with OsRLCK185 in Y2H assay. **b** OsCNGC9 interacts with OsRLCK185 in firefly luciferase complementation assay. **c** In vitro phosphorylation assay showing that the C-terminus of OsCNGC9 (OsCNGC9-C) is phosphorylated by OsRLCK185. **d** Co-immunoprecipitation assay shows that OsCNGC9 interacts with OsRLCK185 in rice protoplasts. **e** Ca^{2+} imaging experiments showing the activation of OsCNGC9 by OsRLCK185 and the consequent increase of $[\text{Ca}^{2+}]_{\text{cyt}}$ in HEK293T cells. Typical fluorescent images (left panel) and average fluorescent intensity changes (right panel) in HEK293T cells transiently expressing various tested proteins as indicated. **f** Chitin induces phosphorylation of OsCNGC9 C-terminus. Kitaake or *OsCERK1-KO-9* protoplasts expressing OsCNGC9-C-FLAG were treated with chitin for 10 min before protein extraction. Total protein was fractionated by SDS-PAGE containing Phos-tag acrylamide (upper panel) and normal SDS-PAGE (lower panel)

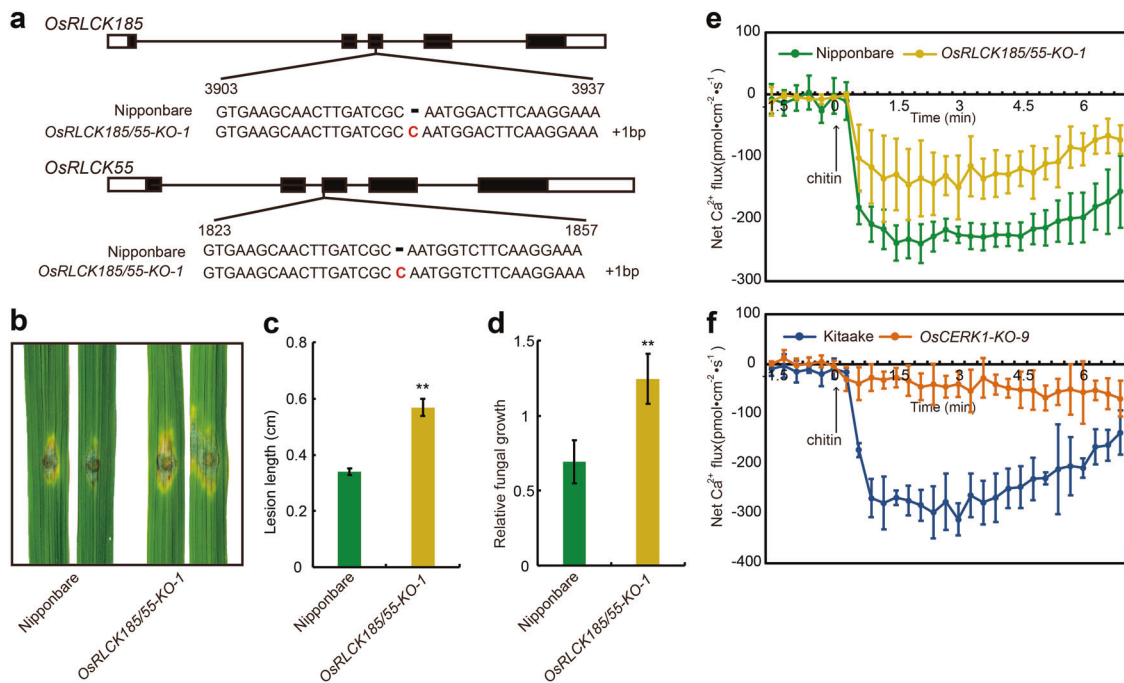


Fig. 5 *Osrlck185/55* double mutant plants show impaired blast resistance and reduced chitin-induced Ca^{2+} influx. **a** Sketch map of the mutations in the knockout line (*Osrlck185/55-KO-1*). Plus (+) sign indicates the number of nucleotides. **b** The *Osrlck185/55* double mutant plants are more susceptible to blast at the seedling stage (blast isolate 2015-412 was used for inoculation). **c**, **d** Lesion length (**c**) and relative fungal growth (**d**) of Nipponbare and *Osrlck185/55* double mutant plants after punch inoculation with the blast. **e** Comparison of calcium influx in mesophyll cells from Nipponbare and *Osrlck185/55* double mutant plants after chitin treatment. **f** Comparison of calcium influx in mesophyll cells from Kitaake and *OsCERK1-KO-9* mutant plants after chitin treatment. Values are means \pm SD (**c**, $n = 10$ samples; **d**, $n = 3$ replicates; **e**, **f**, $n = 6$ replicates). The Student's *t*-test analysis indicates a significant difference (** $P < 0.01$)

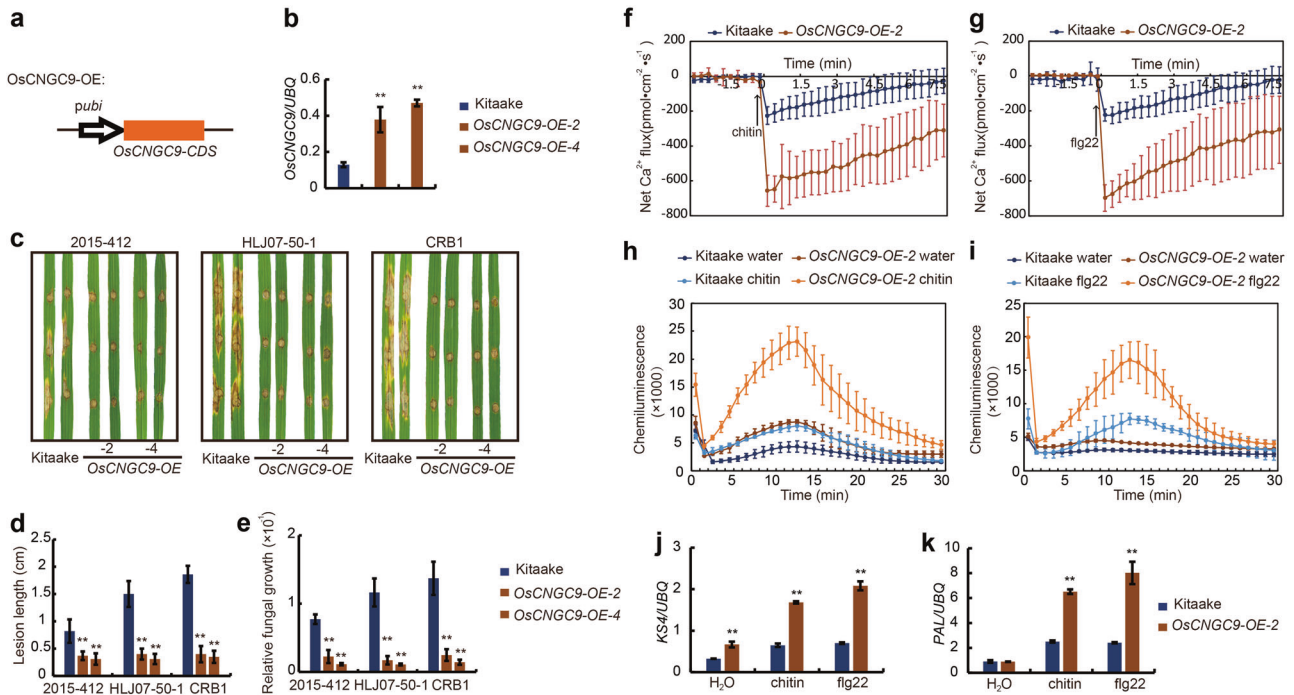


Fig. 6 *OsCNGC9* expression positively regulates rice PTI and blast resistance. **a** Diagram of the *OsCNGC9-OE* construct. *Pubi*, maize *Ubiquitin* promoter; *OsCNGC9-CDS*, the coding sequence of *OsCNGC9*. **b** qRT-PCR measurement of the expression levels of *OsCNGC9* in leaves of Kitaake and the *OsCNGC9-OE* transgenic plants. **c** The *OsCNGC9-OE* transgenic lines confer increased blast resistance. Three blast isolates (2015-412, HLJ07-50-1 and CRB1) were used in the assay. **d, e** Lesion length (**d**) and relative fungal growths (**e**) were recorded in Kitaake and *OsCNGC9-OE* transgenic lines after inoculation with blast isolates. **f, g** Comparison of calcium influx in the mesophyll cells of Kitaake and *OsCNGC9-OE* transgenic plants after chitin (**f**) or flg22 (**g**) treatments. **h, i** Comparison of ROS induction in the leaves of Kitaake and *OsCNGC9-OE* transgenic plants subject to treatment of chitin (**h**) or flg22 (**i**) for 1 h. **j, k** Comparison of the expression levels of *KS4* (**j**) and *PAL* (**k**) after flg22 or chitin treatments in leaves of Kitaake and *OsCNGC9-OE* transgenic plants. Values are means \pm SD (**d**, $n = 10$ samples; **b, e–k**, $n = 3$ replicates). The Student's *t*-test analysis indicates a significant difference (** $P < 0.01$)

OsRLCK185 and its close homologue, OsRLCK55, participate in the regulation of blast resistance and PAMP-induced Ca^{2+} influx in rice.

OsCNGC9 overexpression confers enhanced rice PTI and blast resistance

To evaluate the potential value of *OsCNGC9* in crop genetic improvement, we generated *OsCNGC9* overexpression (*OsCNGC9-OE*) transgenic lines by transforming the coding sequence of *OsCNGC9* under control of the maize *UBIQUITIN* promoter into Kitaake background (Fig. 6a). Two stable transgenic lines with increased levels of the *OsCNGC9* transcripts were identified and selected for further blast resistance assay (Fig. 6b). We found that the *OsCNGC9-OE* lines conferred increased blast resistance to three different blast isolates, compared with the Kitaake (Fig. 6c–e).

Consistently, after PAMPs stimulation, the mesophyll cells of *OsCNGC9-OE* transgenic plants showed stronger Ca^{2+} influx, higher PAMPs-triggered ROS burst and higher levels of PTI-related defense genes expression compared with those of Kitaake plants (Fig. 6f–k). Therefore, we conclude that *OsCNGC9* functions as a rate-limiting positive regulator of rice PTI.

DISCUSSION

In summary, here we identify *OsCNGC9* as a positive regulator of PTI, which acts as a Ca^{2+} -permeable divalent cation-selective inward channel. We further show that *OsCNGC9* channel activity can be activated by OsRLCK185-mediated phosphorylation. Together with the earlier report that OsRLCK185 is phosphorylated by the chitin receptor OsCERK1 during chitin-induced plant immunity,^{12,13} our data collectively suggest a model in which OsCERK1 and OsRLCK185 are activated upon pattern recognition,

leading to phosphorylation and enhancement of *OsCNGC9* channel activity. Then *OsCNGC9*-mediated Ca^{2+} influx triggers a series of immune responses including ROS burst and PTI-related defense genes expression, which ultimately leads to enhanced disease resistance in rice (Fig. 7). In support of this model, we showed that chitin-induced phosphorylation of *OsCNGC9* C-terminus and chitin-induced Ca^{2+} influx were severely impaired in the *Oscerk1* knockout mutant (Figs. 4f, 5f and Supplementary information, Fig. S7f). Moreover, phosphorylation of human CNGC has also been shown to be involved in regulating channel activity.⁴³

It is worth mentioning that besides OsRLCK185, several other OsRLCKs have been shown to be involved in regulation of PTI responses and disease resistance in rice.^{9,18} Their regulatory relationship with OsCERK1 and *OsCNGC9* will be an interesting avenue for future research. In addition, there is also evidence suggesting that the activation of MAPK cascades and anion channel opening are also triggered by pattern recognition.^{9,44} Thus, the relationship between *OsCNGC9*-mediated Ca^{2+} influx and PAMPs-triggered signaling events in immune responses is also worthy investigation in the future. Moreover, we observed that both ROS level and PTI-related gene expression were lower in *cds1* compared to WT without PAMPs treatment (Fig. 3), suggesting that *OsCNGC9* may also play additional roles unrelated to PTI. In line with this, AtCNGC14, a close homologue of *OsCNGC9*, was reported to regulate root development.^{27,45}

Like mutant plants with mutations of many immune protein-coding genes,^{1,34} *cds1* mutant plants display an autoimmunity phenotype including spontaneous PCD, enhanced *PR* gene expression and enhanced disease resistance after flowering (Supplementary information, Fig. S8). Similar phenotypes were also observed in the Arabidopsis *dnd1* mutant, which is defective

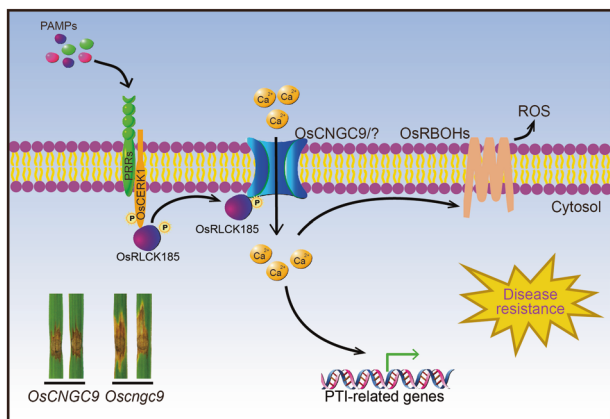


Fig. 7 A proposed model for OsCNGC9 in regulating rice PTI. PAMPs, such as the flg22 and chitin, are sensed by pathogen recognize receptors (PRRs), leading to the activation of OsRLCK185 by OsCERK1.^{12,13} Subsequently, the activated OsRLCK185 phosphorylates OsCNGC9 to enhance its channel activity. The activated OsCNGC9 induces extracellular Ca^{2+} influx and then triggers ROS burst and PTI-related gene expressions, which ultimately leads to enhanced disease resistance in rice. “OsCNGC9/?” represents the potential homomeric and/or heteromeric tetramers that contains OsCNGC9

in *AtCNGC2*.³² It is believed that these proteins have become targets of pathogen effectors during host-pathogen co-evolution. Plant NLR proteins are known to guard these effector targets (guardees) and to initiate immunity when these proteins are post-translationally modified by effectors or altered by genetic lesions in their coding genes.⁴⁶ Thus, the autoimmunity phenotypes of *cds1* plants may result from developmental stage-dependent activation of an unknown NLR that guards OsCNGC9, a possibility to be tested in the future.

Diseases cause significant crop loss, which is a serious threat to global food security. Crop genetic improvement is considered to be a better strategy against diseases than pesticide application that causes environmental pollution. Our result that overexpression of *OsCNGC9* significantly enhanced rice blast resistance (Fig. 6) suggests that precise regulation of *OsCNGC9* expression level may be a useful strategy to balance yield potential and enhanced disease resistance in rice.

MATERIALS AND METHODS

Plant materials and growth conditions

The *cds1* mutant was initially identified from the progenies of a cross between *japonica* Ningjing1 and *japonica* Yun2273, which displayed a cell death phenotype after flowering in the paddy field. Wild type is a normal sibling segregated from the stable progeny of the same cross between *japonica* Ningjing1 and *japonica* Yun2273. The *cds1* mutant, *japonica* Kitaake and Nipponbare were used for further transgenic analysis. All plants including transgenic rice plants were grown in the isolated paddy fields during natural growing seasons at the Chinese Academy of Agricultural Sciences (Beijing) or in a controlled growth chamber (14 h light at 30 °C/10 h darkness at 25 °C, relative humidity of ~80% and light intensity of $\sim 800 \mu\text{mol m}^{-2} \text{s}^{-1}$) for phenotypic analysis and pathogen inoculation.

Blast inoculation on rice leaves

A punch inoculation method with slight modifications was used to inoculate rice plants with blast isolates as described previously.⁴⁷ Briefly, blast isolates were cultured on oat meal agar medium for two weeks for generating spores. Spores were collected by

washing the fungal agar cultures with sterile water (containing 1% Tween 20, Sigma), and the spore concentration of blast isolates was adjusted to $\sim 5 \times 10^5$ spore/ml with sterile water (containing 1% Tween 20) before punch inoculation. Detached leaves of seedling or 7 DAF rice plants were wounded with a hole-punch. 8 μl blast spore suspension was applied to the injured area, and then the inoculated leaves were placed in sterile water that contains 0.1% 6-Benzylaminopurine (Sigma) to keep the moist. The inoculated leaves were kept in darkness at 28 °C for 24 h before they were transferred to a controlled growth chamber (12 h light at 28 °C/12 h darkness at 28 °C). Lesion length was measured using a ruler when significant lesion difference was observed. Relative fungal growth (*MoPot/UBQ*) was measured using qRT-PCR. All primer sequences used here are listed in Supplementary information, Table S2.

Leaf PCD assay

For trypan blue staining assay, leaves of rice plants on 7 DAF were submerged in lactic acid-phenol-Trypan blue solution (25% lactic acid, 23% water-saturated phenol, 0.25% Trypan blue and 25% glycerol) for 48 h. Stained leaf samples were incubated in 70% ethanol until the tissue became clear. For cell death marker gene expression assay, *OsNAC4* was selected as cell death marker gene for detecting leaf PCD level.

The TUNEL assay was performed as described by Xu et al.³⁰ Briefly, leaves were fixed in 4% paraformaldehyde, dehydrated in an ethanol series and embedded in wax. Paraffin-embedded leaves were cut and hydrated and then treated with proteinase K in PBS for 20 min at 37 °C in a humid chamber, followed by rinsing in PBS for three times. The TUNEL assay was conducted with a Dead End Fluorometric TUNEL Kit (Promega) following the manufacturer's instructions. A laser scanning confocal microscope (ZEISS LSM 700) was used to detect the TUNEL signal. The green fluorescence of fluorescein (TUNEL signal) was analyzed at 488 nm (excitation) and 520 nm (detection). The red fluorescence of propidium iodide was analyzed at 488 nm (excitation) and 610 nm (detection).

Map-based cloning

To map the *CDS1* gene, 1,182 mutant individuals were collected from the F_2 population of *cds1* crossed with 9311. The *CDS1* locus was firstly mapped to a 300-kb region on chromosome 9 using 142 F_2 *cds1* individuals by molecular markers. Next, the *cds1* locus was further mapped to a 40-kb region using 1,040 F_2 *cds1* individuals and newly developed molecular markers. PCR and sequencing analysis were employed to identify the candidate gene. All primer sequences used for the map-based cloning procedure are listed in Supplementary information, Table S2.

Plasmid construction and plant transformation

For complementation construct, a 6.5-kb genomic DNA fragment containing the ~ 1.3 -kb promoter region, the entire *OsCNGC9* coding region, and the 1458-bp 3' region was used for vector construction. The fragments were inserted into the binary vector pCambia1305 to generate the pOsCNGC9::OsCNGC9 construct (pGOsCNGC9). Subsequently, the plasmid pGOsCNGC9 was introduced into the *Agrobacterium tumefaciens* strain EHA105 by electroporation and used to infect the calli of *cds1*. Rice transformation was performed as previously described.⁴⁸ For CRISPR (Clustered regularly interspaced short palindromic repeats)/Cas9 construction, a 18-bp gene-specific sequence of *OsCERK1* or a 18-bp common sequence of *OsRLCK185* and *OsRLCK55* was synthesized and annealed to form the oligo adaptors. The oligo adaptors were firstly cloned into the entry vector pOs-sgRNA, and then subcloned into the gateway destination vector pOs-Cas9.⁴⁹ The CRISPR/Cas9 plasmids were introduced into *Agrobacterium tumefaciens* strain EHA105 and then introduced into Kitaake. Positive lines were confirmed by PCR

followed by sequencing. For the *OscNGC9*-OE construct, the full-length CDS of *OscNGC9* was amplified with PCR method. The fragment was then cloned into the pCubi1390 vector to generate the *OscNGC9*-OE construct, which was then introduced into Kitaake using *Agrobacterium*-mediated transformation. All transgenic lines were analyzed using the stable T₂–T₃ progenies. All primer sequences for the constructs are listed in Supplementary information, Table S2.

Promoter activity assay

The promoter activity assay was performed as described previously.⁵⁰ A ~1.3 kb promoter region of *OscNGC9* was cloned into the N-terminus of GUS in the expression vector pCAM-BIA1305.1 to generate the p*OscNGC9*::GUS fusion reporter plasmid, which was introduced into Kitaake by *Agrobacterium*-mediated transformation. Histochemical staining was performed to observe the GUS signal in different tissues and organs in the transgenic plants. Briefly, various tissues of transgenic plants were incubated at 37 °C in a staining solution containing 100 mM NaPO₄ buffer (pH = 7.0), 10 mM Na₂-EDTA, 2 mM X-Gluc, 0.5 mM K₃Fe(CN)₆, 0.5 mM K₄Fe(CN)₆ and 0.1% Triton X-100. After staining, the samples were incubated with 70% ethanol until the tissue became clear. All primer sequences for the constructs are listed in Supplementary information, Table S2.

RNA in situ hybridization

Fully expanded leaves were fixed in RNase-free FAA for 12 h and then dehydrated through an ethanol series. The samples were further embedded in paraffin (Paraplast Plus, Sigma) before sectioning. A cDNA fragment was amplified from the *OscNGC9* coding region and cloned into a pGEM-T vector (Promega) for RNA probe preparation. DIG Northern starter kit (Roche) was used to generate the digoxigenin-labeled RNA probes. In situ hybridization experiments and immunological detection of the signals were performed following the protocol previously described.⁵¹ Slides were observed under bright field using a Leica DMR microscope (Leica DM5000B), and photographed using a camera fitted with a Micro Color CCD (Apogee Instruments). All primer sequences used here are listed in Supplementary information, Table S2.

Phylogenetic analysis

The full-length amino acid sequence of CNGC family proteins, from rice and Arabidopsis were aligned using DNAMAN software (Lynnon BioSoft, Quebec, Canada). The alignment was adjusted manually and the neighbor-joining tree was constructed by MEGA 4.0 (<http://www.megasoftware.net/>) using the bootstrap method with 1000 replicates as previously described.⁵² The amino acid sequences were obtained from Rice Genome Automated Annotation System (<http://ricegaas.dna.affrc.go.jp/>), the Arabidopsis Information Resource (<https://www.arabidopsis.org/>) and the National Center for Biotechnology Information (<https://www.ncbi.nlm.nih.gov/>).

Subcellular localization assay

The subcellular localization assay in rice plants was performed as described previously.⁵³ The promoter region and the full-length CDS of *OscNGC9* were cloned into the pCAMBIA1305-GFP vector to generate the p*OscNGC9*::*OscNGC9*-GFP construct for plant transformation. Transgenic roots were used to analyze the subcellular localization of *OscNGC9*-GFP fusion protein. The subcellular localization of *OscNGC9* protein in rice protoplasts was performed as described previously.⁵⁴ The full-length CDS of *OscNGC9* was cloned into pA7-GFP vector to form *OscNGC9*-GFP fusion protein. A previously characterized plasma membrane protein, PIP2;1 fused with mCherry was used as a plasma membrane marker.⁵⁵ Both constructs were co-transformed into rice protoplasts for subcellular localization analysis. Images were captured using scanning confocal microscope (ZEISS LSM 700). All

primer sequences used here are listed in Supplementary information, Table S2.

Protein interaction assay

The Y2H assay was used to detect protein interaction following the DUALhunter system (Dualsystems Biotech). The full coding sequences of the corresponding genes were fused to the Nub fragment in the pXGY17 vector or to the Cub fragment in the pXGY18 vector, respectively. The process of Y2H assay was conducted according to the method previously described.³⁰

For BiFC assay, the full-length coding sequence of *OscNGC9* was cloned into the binary BiFC vectors pSPYNE173 or pSPYCE(M), respectively. The experiment was conducted as previously described.⁵⁶ Rice GW5 and GSK2 combination was used as a positive control in the BiFC assay.⁵⁷

The luciferase complementation assay was performed in *N. benthamiana* leaves as previously described.⁵⁸ *Agrobacterium* cells harboring the nLUC and cLUC constructs were co-infiltrated into *N. benthamiana* leaves. Leaves were taken 2 days later, incubated with 1 mM luciferin, and the LUC activity was measured by the NightSHADE LB 985 (Berthold). The interactions with GW5 were used as negative controls in the LUC assay.

For Co-IP assay, protoplasts isolated from WT plants were transfected with desired plasmids, incubated overnight. Total protein was extracted with protein extraction buffer (150 mM KCl, 50 mM HEPES [pH7.5], 0.4% Triton-X 100, 1 mM DTT and proteinase inhibitor cocktail). The process of Co-IP assay was conducted as previously described.⁵⁹ Western blots were performed with the anti-HA (CW0092M, CWBIO), anti-GFP (11814460001, Roche), and anti-Mouse secondary antibody (D330, MBL) antibodies. All primer sequences for the constructs are listed in Supplementary information, Table S2.

In vitro phosphorylation assay

For phosphorylation assay, an in vitro phosphorylation assay method with slight modifications was used.⁶⁰ Briefly, HIS- and MBP-tagged recombinant proteins were expressed in *Escherichia coli* strain BL21 and purified according to the user's manual, respectively. Phosphorylation assays were performed with purified beads containing *OscNGC9*-C-MBP and purified HIS-kinases in 30 µl of kinase buffer (40 mM HEPES [pH 7.5], 20 mM MgCl₂, 2 mM DTT, 10 µCi [³²P]γATP, proteinase inhibitor cocktail and phosphatase inhibitor cocktail) for 90 min at 30 °C, and the reaction was stopped by adding SDS loading buffer. After separation on a 10% SDS–polyacrylamide gel, the gel was stained with Coomassie blue. Then, the gel was exposed to GE Amersham hyperfilm MP film for detecting phosphorylated proteins.

Phos-Tag assays

Phos-tag assay was carried out as previously described.⁶¹ Kitaake and *Oscerk1* mutant protoplasts expressing *OscNGC9*-C-FLAG were treated with chitin for 10 min, and proteins were extracted with protein extraction buffer. The samples were subsequently analyzed using 10% SDS–polyacrylamide gels with or without 100 µM MnCl₂ and 50 µM Phos-tag Acrylamide AAL-107 (NARD Institute), respectively. The samples were then transferred to NC membranes, followed by immunoblot analysis with the anti-FLAG (M185-7, MBL) and anti-HSP82 (AbM51099-31-PU, Beijing Protein Innovation) antibodies.

Ion accumulation of *E. coli* assay

Ion accumulation of *E. coli* assay was carried out as previously described with minor modifications.²³ Briefly, the full-length coding sequence of *OscNGC9* fused with GFP was cloned into PET-30a expression vector (Novagen), and the full-length coding sequence of GFP cloned into PET-30a vector was used as the control. The plasmids were separately transformed into *E. coli* strain DE3 (TransGen Biotech). GFP fluorescence was captured

after induction with 0.5 mM isopropyl β -D-thiogalactoside (IPTG) in a *E. coli* bacterial incubation medium containing 2 \times YT medium with 1.6% Tryptone (OXOID) and 1% Yeast extract (OXOID). After induction, *E. coli* cells were collected by centrifugation, pelleted, resuspended in 2% lactose solution and incubated in 2% lactose solution containing 1 mM CaCl_2 , 1 mM RbCl and 1 mM NaCl . After incubation, *E. coli* cells were collected, washed with 2% lactose solution, and digested in HNO_3 overnight. An inductively coupled plasma atomic emission spectroscopy (Varian, Palo Alto, CA) was used for the ion accumulation assay. All primer sequences for the constructs are listed in Supplementary information, Table S2.

Whole-cell patch clamp recordings

OscNGC9-mediated Ca^{2+} and K^+ current recordings in HEK293T cells were performed as described previously.²⁴ Briefly, an Axopatch-200B patch clamp setup (Axon Instruments, CA, USA) and a Digidata 1440A digitizer combined to an Olympus IX71 inverted microscope (Japan) were used for whole cell patch clamp experiments. Patch clamping data was acquired and analyzed using the software pClamp10.2 (Axon Instruments, CA, USA). For Ca^{2+} current recordings in HEK293T cells, the standard bath solution contains 120 mM NaCl , 10 mM CsCl , 10 mM CaCl_2 , 10 mM HEPES, 2.8 mM KCl and 2 mM MgCl_2 and the pH was adjusted to 7.2 with NaOH . The standard pipette solution contains 120 mM Cs-glutamate , 10 mM HEPES, 8 mM NaCl , 6.7 mM EGTA, 3.35 mM CaCl_2 , 3 mM MgCl_2 and 2.5 mM Mg-ATP added freshly each day, and the pH was adjusted to 7.2 with CsOH . The free Ca^{2+} concentration was 175 nM calculated by the online free software Webmaxc Standard (<http://www.stanford.edu/~cpatton/webmaxc/webmaxc5.htm>). The osmolality of bath and pipette solutions was adjusted to 313.3 mmol/kg with D-glucose. For inward K^+ current recordings, the bath solution contains 120 mM NaCl , 14.5 mM KCl , 10 mM glucose, 10 mM HEPES, 2 mM CaCl_2 and 1 mM MgCl_2 and the pH was adjusted to 7.2 with NaOH . The pipette solution contains 145 mM K-glutamate , 10 mM HEPES, 8 mM Na-glutamate , 4 mM Mg-glutamate , 3.35 mM EGTA, 1.675 mM CaCl_2 and the pH was adjusted to 7.2 with NaOH . The free Ca^{2+} concentration was 100 nM calculated by the online free software Webmaxc Standard. The osmolality of bath and pipette solutions for K^+ current recordings was adjusted with D-glucose to 313.3 mmol/kg. primer sequences for the vector construction are listed in Supplementary information, Table S2.

Calcium imaging assay

Free calcium imaging assay in HEK293T cells was performed as described previously with minor modifications.⁶² Briefly, the full-length CDS of *OscNGC9* with *YC3.6* fused to its C terminus or the full-length CDS of *OsRLCK185* (*OsRLCK185-K108E*) with mCherry fused to its C terminus was cloned into the pCI-neo vector. The kinase inactive mutant of *OsRLCK185*, *OsRLCK185-K108E* was designed according to the method previously described.¹² *YC3.6* fluorescence was observed under an inverted microscope (D1, Carl Zeiss, Germany) for monitoring the ratio (535 nm/480 nm) of *YC3.6*. MAG Biosystems 7.5 software (MetaMorph, USA) was used for data acquisition and analysis, and the interval of data acquisition was 9 s. The standard external working solution for Ca^{2+} imaging contained 120 mM NaCl , 10 mM Glucose, 10 mM HEPES, 3 mM KCl , 1.2 mM NaHCO_3 and 1 mM MgCl_2 , pH 7.2 adjusted with NaOH , and external Ca^{2+} was added as indicated. All primer sequences for vector construction are listed in Supplementary information, Table S2.

Measurements of net Ca^{2+} flux

Net Ca^{2+} flux was measured using Non-invasive Micro-test Technique (NMT-YG-100, YoungerUSA LLC, Amherst, MA01002, USA) as previously described with minor modifications.⁶³ Leaves sampled from rice seedling were immobilized in the measuring buffer (0.2 mM CaCl_2 , 0.1 mM NaCl , 0.1 mM MgCl_2 and 0.1 mM KCl ,

pH 5.2) for 30 min equilibration. Then the steady-state fluxes in leaf mesophyll cells were continuously recorded for 5 min prior to the PAMPs treatments. Chitin (Santa Cruz Biotechnology) or flg22 (ANASPEC PEPTIDE) peptide was slowly added to the measuring buffer until the chitin concentration reached 10 μM , or the flg22 concentration reached 10 μM . Afterward, transient flux of Ca^{2+} was recorded and continued for 10 min.

Detection of ROS bursts

The detection of ROS bursts was conducted as previously described.⁶⁴ Leaf disks were obtained from fully expanded leaves of rice plants using an ear-hole puncher and floated on ddH_2O for 12 h. Three disks were placed in a 1.5-ml microcentrifuge tube that contains 100 μl of luminol (Bio-Rad Immun-Star horseradish peroxidase substrate 170-5040) and 1 μl horseradish peroxidase (Jackson Immuno Research) and flg22 or chitin, with ddH_2O for the control. The tube was immediately measured in a Glomax 20/20 luminometer (Promega) at 15 s intervals over a period of 30 min.

Detection of PTI-related genes expression

The detection of PTI-related genes expression was conducted as previously described with minor modifications.⁶⁵ Leaves of rice seedlings were cut to 3 mm strips. The materials were floated on water overnight to recover from wounding stress. Afterward, materials were then treated with water (mock), flg22 peptide or chitin for 1 h followed by freezing in liquid nitrogen. Materials were used for RNA isolation and qRT-PCR assay. The primer sequences for qRT-PCR assay are listed in Supplementary information, Table S2.

RNA isolation and qRT-PCR assay

The RNA isolation and qRT-PCR assay were conducted as previously described.⁵² Briefly, total RNA was extracted from rice tissues using a plant RNA extraction kit (Qiagen, Hilden, Germany) according to the manufacturer's instructions. For qRT-PCR, total RNA (1 μg) was reverse transcribed to cDNA using a QuantiTect Reverse Transcription Kit (Qiagen). The qRT-PCR assay was performed using a SYBR Premix Ex TaqTM kit (TaKaRa) and an ABI prism 7500 Real-Time PCR System. The primer sequences for qRT-PCR assay are listed in Supplementary information, Table S2.

ACKNOWLEDGEMENTS

We thank Drs. Guo-Liang Wang, Yue-se Ning and Xuetao Shi for technical assistance in ROS detection; Drs. Xiaojuan Zhang, Weibing Wang and Jiafan Liu for help in phosphorylation assay. This work was supported by the National Key R&D Program of China (2017YFD0100404 and 2016YFD0100600) and National Natural Science Foundation of China (31471758).

AUTHOR CONTRIBUTIONS

Jiachang W., X.L. and A.Z. designed and performed most of the experiments. Y.X., Fan W. and Yihua W. performed genetic analysis and mapping. Yan-Qiu T. and Yong-Fei W. performed the electrophysiological assay. C.L., J.L., S.W., L.M. and H.Z. performed blast inoculation and subcellular localization assay. T.P., Yongfei W. and C.Z. performed protein-protein interaction assay. Xin Z., X.G., L.J., Yupeng W., X.J., Sheng L. and Xiao Z. performed construction and genetic transformation. G. W., X.C. and E. W. constructed the *Osrlck185/55* double mutant plants. S.Z., Y.R., Q.L., C.W., Z.C., Jiulin W., Yunlu T. and Shijia L. provided technical help with experiments. Jiachang W., Y.R. and Fuqing W. drafted the manuscript. Jianmin W., J.Z. and H.W. supervised the project and revised the manuscript.

ADDITIONAL INFORMATION

Supplementary information accompanies this paper at <https://doi.org/10.1038/s41422-019-0219-7>.

Competing interests: The authors declare no competing interests.

REFERENCES

- Jones, J. D. & Dangl, J. L. The plant immune system. *Nature* **444**, 323–329 (2006).
- Boller, T. & He, S. Y. Innate immunity in plants: an arms race between pattern recognition receptors in plants and effectors in microbial pathogens. *Science* **324**, 742–744 (2009).
- Spoel, S. H. & Dong, X. N. How do plants achieve immunity? Defence without specialized immune cells. *Nat. Rev. Immunol.* **12**, 89–100 (2012).
- Couto, D. & Zipfel, C. Regulation of pattern recognition receptor signalling in plants. *Nat. Rev. Immunol.* **16**, 537–552 (2016).
- Thor, K. & Peiter, E. Cytosolic calcium signals elicited by the pathogen-associated molecular pattern flg22 in stomatal guard cells are of an oscillatory nature. *New Phytol.* **204**, 873–881 (2014).
- Dodd, A. N., Kudla, J. & Sanders, D. The language of calcium signaling. *Annu. Rev. Plant Biol.* **61**, 593–620 (2010).
- Boudsocq, M. et al. Differential innate immune signalling via Ca²⁺ sensor protein kinases. *Nature* **464**, 418–422 (2010).
- Yuan, P. G., Jauregui, E., Du, L. Q., Tanaka, K. & Poovaiah, B. W. Calcium signatures and signaling events orchestrate plant–microbe interactions. *Curr. Opin. Plant Biol.* **38**, 173–183 (2017).
- Liang, X. & Zhou, J. M. Receptor-like cytoplasmic kinases: central players in plant receptor kinase-mediated signaling. *Annu. Rev. Plant Biol.* **69**, 267–299 (2018).
- Li, L. et al. The FLS2-associated kinase BIK1 directly phosphorylates the NADPH oxidase RbohD to control plant immunity. *Cell Host Microbe* **15**, 329–338 (2014).
- Ao, Y. et al. OsCERK1 and OsRLCK176 play important roles in peptidoglycan and chitin signaling in rice innate immunity. *Plant J.* **80**, 1072–1084 (2014).
- Yamaguchi, K. et al. A receptor-like cytoplasmic kinase targeted by a plant pathogen effector is directly phosphorylated by the chitin receptor and mediates rice immunity. *Cell Host Microbe* **13**, 347–357 (2013).
- Wang, C. et al. OsCERK1-mediated chitin perception and immune signaling requires receptor-like cytoplasmic kinase 185 to activate a MAPK cascade in rice. *Mol. Plant* **10**, 619–633 (2017).
- Dean, R. A. et al. The genome sequence of the rice blast fungus *Magnaporthe grisea*. *Nature* **434**, 980–986 (2005).
- Deng, Y. et al. Epigenetic regulation of antagonistic receptors confers rice blast resistance with yield balance. *Science* **355**, 962–965 (2017).
- Liu, W., Liu, J., Triplett, L., Leach, J. E. & Wang, G. L. Novel insights into rice innate immunity against bacterial and fungal pathogens. *Annu. Rev. Phytopathol.* **52**, 213–241 (2014).
- Chen, X. & Ronald, P. C. Innate immunity in rice. *Trends Plant Sci.* **16**, 451–459 (2011).
- Fan, J. et al. The monocot-specific receptor-like kinase SDS2 controls cell death and immunity in rice. *Cell Host Microbe* **23**, 498–510 (2018).
- You, Q. et al. An E3 ubiquitin ligase-BAG protein module controls plant innate immunity and broad-spectrum disease resistance. *Cell Host Microbe* **20**, 758–769 (2016).
- Zagotta, W. N. & Siegelbaum, S. A. Structure and function of cyclic nucleotide-gated channels. *Annu. Rev. Neurosci.* **19**, 235–263 (1996).
- Leng, Q., Mercier, R. W., Hua, B. G., Fromm, H. & Berkowitz, G. A. Electrophysiological analysis of cloned cyclic nucleotide-gated ion channels. *Plant Physiol.* **128**, 400–410 (2002).
- Leng, Q., Mercier, R. W., Yao, W. & Berkowitz, G. A. Cloning and first functional characterization of a plant cyclic nucleotide-gated cation channel. *Plant Physiol.* **121**, 753–761 (1999).
- Frietsch, S. et al. A cyclic nucleotide-gated channel is essential for polarized tip growth of pollen. *Proc. Natl Acad. Sci. USA* **104**, 14531–14536 (2007).
- Gao, Q. et al. *Arabidopsis* CNGC18 is a Ca²⁺-permeable channel. *Mol. Plant* **7**, 739–743 (2014).
- Gao, Q. et al. Cyclic nucleotide-gated channel 18 is an essential Ca²⁺ channel in pollen tube tips for pollen tube guidance to ovules in *Arabidopsis*. *Proc. Natl Acad. Sci. USA* **113**, 3096–3101 (2016).
- Pan, Y. et al. Dynamic interactions of plant CNGC subunits and calmodulins drive oscillatory Ca²⁺ channel activities. *Dev. Cell* **48**, 710–725 (2019).
- Shih, H. W., DePew, C., Miller, N. & Monshausen, G. The cyclic nucleotide-gated channel CNGC14 regulates root gravitropism in *Arabidopsis thaliana*. *Curr. Biol.* **25**, 3119–3125 (2015).
- Wang, Y. et al. Identification of cyclic GMP-activated nonselective Ca²⁺-permeable cation channels and associated CNGC5 and CNGC6 genes in *Arabidopsis* guard cells. *Plant Physiol.* **163**, 578–590 (2013).
- Wang, Y. et al. CNGC2 is a Ca²⁺ influx channel that prevents accumulation of apoplastic Ca²⁺ in the leaf. *Plant Physiol.* **173**, 1342–1354 (2017).
- Xu, Y. et al. OsCNGC13 promotes seed-setting rate by facilitating pollen tube growth in stylar tissues. *PLoS Genet.* **13**, e1006906 (2017).
- DeFalco, T. A., Moeder, W. & Yoshioka, K. Opening the gates: insights into cyclic nucleotide-gated channel-mediated signaling. *Trends Plant Sci.* **21**, 903–906 (2016).
- Yu, I. C., Parker, J. & Bent, A. F. Gene-for-gene disease resistance without the hypersensitive response in *Arabidopsis dnd1* mutant. *Proc. Natl Acad. Sci. USA* **95**, 7819–7824 (1998).
- Yoshioka, K. et al. Environmentally sensitive, SA-dependent defense responses in the *cpr22* mutant of *Arabidopsis*. *Plant J.* **26**, 447–459 (2001).
- Rodriguez, E., El Ghoul, H., Mundy, J. & Petersen, M. Making sense of plant autoimmunity and ‘negative regulators’. *FEBS J.* **283**, 1385–1391 (2016).
- Nawaz, Z., Kakar, K. U., Saand, M. A. & Shu, Q. Y. Cyclic nucleotide-gated ion channel gene family in rice, identification, characterization and experimental analysis of expression response to plant hormones, biotic and abiotic stresses. *BMC Genom.* **15**, 853 (2014).
- Chiasson, D. M. et al. A quantitative hypermorphic CNGC allele confers ectopic calcium flux and impairs cellular development. *eLife* **6**, e25012 (2017).
- Schachtman, D. P., Schroeder, J. I., Lucas, W. J., Anderson, J. A. & Gaber, R. F. Expression of an inward-rectifying potassium channel by the *Arabidopsis* KAT1 cDNA. *Science* **258**, 1654–1658 (1992).
- Chinchilla, D. et al. A flagellin-induced complex of the receptor FLS2 and BAK1 initiates plant defence. *Nature* **448**, 497–500 (2007).
- Wan, J. et al. A LysM receptor-like kinase plays a critical role in chitin signaling and fungal resistance in *Arabidopsis*. *Plant Cell* **20**, 471–481 (2008).
- Ranf, S., Eschen-Lippold, L., Pecher, P., Lee, J. & Scheel, D. Interplay between calcium signalling and early signalling elements during defence responses to microbe- or damage-associated molecular patterns. *Plant J.* **68**, 100–113 (2011).
- Ranf, S. et al. Microbe-associated molecular pattern-induced calcium signaling requires the receptor-like cytoplasmic kinases, PBL1 and BIK1. *BMC Plant Biol.* **14**, 374 (2014).
- Shiu, S. H. et al. Comparative analysis of the receptor-like kinase family in *Arabidopsis* and rice. *Plant Cell* **16**, 1220–1234 (2004).
- Zong, X. et al. A novel mechanism of modulation of hyperpolarization-activated cyclic nucleotide-gated channels by Src kinase. *J. Biol. Chem.* **280**, 34224–34232 (2005).
- Jeworutzki, E. et al. Early signaling through the *Arabidopsis* pattern recognition receptors FLS2 and EFR involves Ca-associated opening of plasma membrane anion channels. *Plant J.* **62**, 367–378 (2010).
- Dindas, J. et al. AUX1-mediated root hair auxin influx governs SCF^{TIR1/AFB}-type Ca²⁺ signaling. *Nat. Commun.* **9**, 1174 (2018).
- Lolle, S. et al. Matching NLR immune receptors to autoimmunity in *camta3* mutants using antimorphic NLR alleles. *Cell Host Microbe* **21**, 518–529 (2017).
- Li, W. et al. A natural allele of a transcription factor in rice confers broad-spectrum blast resistance. *Cell* **170**, 114–126 (2017).
- Hiei, Y., Ohta, S., Komari, T. & Kumashiro, T. Efficient transformation of rice (*Oryza sativa* L.) mediated by *Agrobacterium* and sequence analysis of the boundaries of the T-DNA. *Plant J.* **6**, 271–282 (1994).
- Miao, J. et al. Targeted mutagenesis in rice using CRISPR-Cas system. *Cell Res.* **23**, 1233–1236 (2013).
- Zhou, F. et al. D14-SCF^{D3}-dependent degradation of D53 regulates strigolactone signalling. *Nature* **504**, 406–410 (2013).
- Tan, J. et al. *OsCOL10*, a *CONSTANS*-Like gene, functions as a flowering time repressor downstream of *Ghd7* in rice. *Plant Cell Physiol.* **57**, 798–812 (2016).
- Wang, J. et al. Overexpression of OsMYB1R1-VP64 fusion protein increases grain yield in rice by delaying flowering time. *FEBS Lett.* **590**, 3385–3396 (2016).
- Zhu, S. et al. The OSHAPL1-DTH8-Hd1 complex functions as the transcription regulator to repress heading date in rice. *J. Exp. Bot.* **68**, 553–568 (2017).
- Yu, X. et al. A selfish genetic element confers non-Mendelian inheritance in rice. *Science* **360**, 1130–1132 (2018).
- Lee, H. et al. Drought stress-induced Rma1H1, a RING membrane-anchor E3 ubiquitin ligase homolog, regulates aquaporin levels via ubiquitination in transgenic *Arabidopsis* plants. *Plant Cell* **21**, 622–641 (2009).
- Ren, Y. et al. *GLUTELIN PRECURSOR ACCUMULATION3* encodes a regulator of post-Golgi vesicular traffic essential for vacuolar protein sorting in rice endosperm. *Plant Cell* **26**, 410–425 (2014).
- Liu, J. et al. GW5 acts in the brassinosteroid signalling pathway to regulate grain width and weight in rice. *Nat. Plants* **3**, 17043 (2017).
- Liu, J. et al. MicroRNA319-regulated TCPs interact with FBHs and PFT1 to activate CO transcription and control flowering time in *Arabidopsis*. *PLoS Genet.* **13**, e1006833 (2017).
- Liang, X. et al. Ligand-triggered de-repression of *Arabidopsis* heterotrimeric G proteins coupled to immune receptor kinases. *Cell Res.* **28**, 529–543 (2018).
- Lin, Q. et al. The SnRK2-APC/C^{TE} regulatory module mediates the antagonistic action of gibberellic acid and abscisic acid pathways. *Nat. Commun.* **6**, 7981 (2015).

61. Bi, G. et al. Receptor-like cytoplasmic kinases directly link diverse pattern recognition receptors to the activation of mitogen-activated protein kinase cascades in *Arabidopsis*. *Plant Cell* **30**, 1543–1561 (2018).
62. Yang, D. et al. Calcium pumps and interacting BON1 protein modulate calcium signature, stomatal closure, and plant immunity. *Plant Physiol.* **175**, 424–437 (2017).
63. Ma, Y. et al. *COLD1* confers chilling tolerance in rice. *Cell* **160**, 1209–1221 (2015).
64. Shi, X. et al. The fungal pathogen *Magnaporthe oryzae* suppresses innate immunity by modulating a host potassium channel. *PLoS Pathog.* **14**, e1006878 (2018).
65. Park, C. H. et al. The *Magnaporthe oryzae* effector AvrPiz-t targets the RING E3 ubiquitin ligase APIP6 to suppress pathogen-associated molecular pattern-triggered immunity in rice. *Plant Cell* **24**, 4748–4762 (2012).